AGU PUBLICATIONS

JGR

Journal of Geophysical Research: Atmospheres

RESEARCH ARTICLE
10.1002/2017JD026950

Key Points:
- The kinetic isotope effect (KIE) for C_2H_6 + OH was experimentally derived in the range 243-303 K, yielding improved measurement precision
- The KIE temperature dependence was also determined theoretically using quantum chemistry combined with transition state theory
- Both laboratory observations and theoretical calculations showed no significant KIE temperature dependence

Supporting Information:
- Supporting Information S1
- Data Set S1
- Data Set S2

Correspondence to:
I. Gensch and L. Vereecken,
i.gensch@fz-juelich.de;
l.vereecken@fz-juelich.de

Citation:
Piansawan, T., M. Saccon, L. Vereecken, I. Gensch, and A. Kiendler-Scharr (2017), Temperature dependence of stable carbon kinetic isotope effect for the oxidation reaction of ethane by OH radicals: Experimental and theoretical studies, *J. Geophys. Res. Atmos.*, *122*, 8310–8324, doi:10.1002/2017JD026950.

Received 11 APR 2017
Accepted 12 JUL 2017
Accepted article online 15 JUL 2017
Published online 5 AUG 2017

Temperature dependence of stable carbon kinetic isotope effect for the oxidation reaction of ethane by OH radicals: Experimental and theoretical studies

T. Piansawan[1], M. Saccon[2], L. Vereecken[1], I. Gensch[1], and A. Kiendler-Scharr[1]

[1]Institute of Energy and Climate Research (IEK-8), Forschungszentrum Jülich, Jülich, Germany, [2]Centre for Atmospheric Chemistry, York University, Toronto, Ontario, Canada

Abstract The stable carbon kinetic isotope effect (KIE) of ethane photooxidation by OH radicals was deduced by employing both laboratory measurements and theoretical calculations. The investigations were designed to elucidate the temperature dependence of KIE within atmospherically relevant temperature range. The experimental KIE was derived from laboratory compound-specific isotope analyses of ethane with natural isotopic abundance exposed to OH at constant temperature, showing ε values of 7.16 ± 0.54‰ (303 K), 7.45 ± 0.48‰ (288 K), 7.36 ± 0.28‰ (273 K), 7.61 ± 0.28‰ (263 K), 8.89 ± 0.90‰ (253 K), and 9.42 ± 2.19‰ (243 K). Compared to previous studies, a significant improvement of the measurement precision was reached at the high end of the investigated temperature range. The KIE was theoretically determined as well, in the temperature range of 150 K to 400 K, by calculating the reaction rate coefficients of ^{12}C and singly ^{13}C substituted ethane isotopologues applying chemical quantum mechanics together with transition state theory. Tunneling effect and internal rotations were also considered. The agreement between experimental and theoretical results for rate coefficients and KIE in an atmospherically relevant temperature range is discussed. However, both laboratory observations and computational predictions show no significant temperature dependence of the KIE for the ethane oxidation by OH radicals.

1. Introduction

Ethane (C_2H_6) is the most abundant non-methane hydrocarbon in the atmosphere, impacting on air quality, human health, and climate [*Schultz et al.*, 2015]. Major emission sources of ethane are associated with the extraction, transmission, and processing of oil and gas, as well as the combustion of fossil fuels and biomass [*Etiope and Ciccioli*, 2009; *Gupta et al.*, 1998; *Pozzer et al.*, 2010; *Rudolph*, 1995; *Simpson et al.*, 2012; *Xiao et al.*, 2008]. The most significant atmospheric ethane sink is its oxidation by hydroxyl radicals (OH). The reaction rate coefficient, k_{OH} is 2.4×10^{-13} cm^3 molecule^{-1} s^{-1} at 298 K [*Atkinson et al.*, 2006]. With a mean atmospheric lifetime of approximately 2 months at an average OH concentration of 10^6 molecules cm^{-3} [*Gupta et al.*, 1998; *Pozzer et al.*, 2010; *Rudolph*, 1995], ethane is considered a relatively long-lived chemical species, accumulating in the troposphere and, thus, influencing the photochemistry on hemispheric scales. The quantification of the ethane impact requires an accurate knowledge of its sources and processing through atmospheric transport.

Stable carbon isotopic ratio investigations, complementarily to concentration measurements, were demonstrated to give more insight in source apportionment and the atmospheric processing of organic compounds [*Gensch et al.*, 2014; *Goldstein and Shaw*, 2003]. Stable isotopic composition measurements together with knowledge of the kinetic isotope effect (KIE) can be used to evaluate the chemical age of an air mass. Conceptually, the application of stable isotopes makes use of the properties of two coemitted tracers. In this case, the heavy isotopologue of the investigated species—containing at least one ^{13}C—and the light one—with ^{12}C only—are coemitted with the same emission factor. In addition, due to the KIE, the corresponding rate coefficients of their oxidation reactions are only slightly different. Therefore, quantifying the extent of oxidative loss of an individual compound can be achieved from observed changes in its isotopic composition from emission to the point of observation according to the "isotopic hydrocarbon clock" [*Rudolph and Czuba*, 2000]. Moreover, isotopes provide source "fingerprints," i.e., trace gases emitted from different sources have a specific isotopic composition, the so called "isotopic signature" [*Jenden and Kaplan*, 1986; *Rudolph et al.*, 1997, 2002]. They "footprint" the atmospheric processing, since the isotope effects are reaction specific. Thus, isotopic analyses can differentiate between mixing and chemical loss processes [*Nara et al.*, 2007; *Saito et al.*, 2002].

In the last two decades, the pool of information on ethane source-specific stable carbon isotope ratios and ambient concentrations and $\delta^{13}C$ steadily increased [*Nara et al.*, 2007; *Rudolph*, 1995; *Rudolph et al.*, 1997, 2002; *Saito et al.*, 2002, 2009; *Tsunogai et al.*, 1999]. These were used as input in 3-D chemical modeling studies on the global isotopic distribution for ethane [*Saito et al.*, 2011; *Stein and Rudolph*, 2007; *Thompson et al.*, 2003] together with a KIE value of 8.57 ± 1.95‰ [*Anderson et al.*, 2004], which was experimentally derived at room temperature (296 ± 4 K) for the ethane + OH reaction. In their simulations, *Thompson et al.* [2003] kept the source $\delta^{13}C_0$ constant. Later, *Stein and Rudolph* [2007] and *Saito et al.* [2011] differentiated the emission isotopic composition based on source type. By comparing model results with ambient observations of ethane mixing ratios and $\delta^{13}C$, they could confirm the missing ethane sources indicated by *Thompson et al.* [2003]. In addition, they could provide some indirect evidence for the type, as well as the magnitude and latitude range of the unidentified sources. Both studies indicated that the implemented KIE value of 8.57 ± 1.95‰ might be too high. A reduction of approximately 3‰ would deliver a better agreement between the modeled and observed $\delta^{13}C$ values.

Quantum chemical modeling with theoretical kinetic calculations has treated the stable carbon KIEs by calculating the ratio of the reaction rate coefficients for each isotopologue. Due to the subtle changes introduced by ^{13}C substitution, these calculations have stringent requirements on the level of theory used and concomitantly an expensive computational cost [*Barker et al.*, 2012; *Fast et al.*, 1998; *Gonzalez-Lafont et al.*, 1998; *Villa et al.*, 1999]. Typically, only small systems, such as methane oxidations, were investigated [*Barker et al.*, 2012; *Lin et al.*, 2005; *Sellevåg et al.*, 2006; *Tanaka et al.*, 1996], where more recent studies introduce improved descriptions of tunneling, anharmonicity, internal rotations, etc. for better predictions.

The overall goal of this experimental work is to accurately examine the KIE of the ethane oxidation reaction by OH at room temperature. For consistency, the KIE temperature dependence is investigated, too. The main focus of this study is to improve the measurement precision, in spite of the challenging experimental conditions, such as long chemical lifetime of ethane. In addition, this study aims to theoretically investigate the KIE. Since the ethane + OH reaction is a relatively small system, the theoretical studies strive to use a high level of theory according to the available computational power. As a result, we expect to have molecular level insights into its reaction kinetics. Furthermore, the theoretical investigations aim to cover atmospheric temperature ranges, where experimental work has strong limitations.

2. Stable Carbon Isotope Ratios in Atmospheric Studies

In samples from different sources, naturally occurring differences in the stable carbon isotope ratios ($^{13}C/^{12}C$) are very small, and therefore, these are expressed using the delta notation, in per mill (‰):

$$\delta^{13}C_{\text{sample}} = \left(\frac{\left(^{13}C\,/^{12}C\right)_{\text{sample}}}{\left(^{13}C\,/^{12}C\right)_{\text{standard}}} - 1 \right) \cdot 1000/‰ \tag{1}$$

In this work, the reported $\delta^{13}C$ values of the investigated samples are given relatively to the internationally accepted reference standard, Vienna Peedee belemnite (VPDB) [*Brand et al.*, 2010].

Due to the isotopic substitution, the reaction rate of isotopologues changes slightly translating in a kinetic isotope effect. The stable carbon KIE value is defined as follows:

$$KIE = \frac{k_{12}}{k_{13}} \tag{2}$$

where k_{12} is the rate coefficient of a reaction in which the reactant contains solely ^{12}C atoms and k_{13} is that of a reaction involving at least one ^{13}C atom. Both coefficients are temperature dependent. Isotope fractionation effects are generally very small. Therefore, the KIE, which is very close to unity, is expressed in per mill (‰) epsilon notation:

$$\varepsilon = \left(\frac{k_{12}}{k_{13}} - 1 \right) \cdot 1000‰ = \quad (KIE - 1) \cdot 1000‰ \tag{3}$$

In laboratory, the KIE of a reaction can be determined from concentration and $\delta^{13}C$ measurements as a function of reaction time [*Rudolph*, 2007]. Explicitly, when using the relative rate approach for ^{13}C and ^{12}C, a relationship between concentration and isotopic ratios during the reaction is derived:

$$\ln\frac{\left[{}^{12}C\right]_t}{\left[{}^{12}C\right]_0} = \frac{KIE}{1-KIE}\ \ln\frac{\delta^{13}C_t + 1000}{\delta^{13}C_0 + 1000} \tag{4}$$

where $[^{12}C]_t$ and $[^{12}C]_0$ denote the reactant concentration at time t and $t = 0$, respectively.

The oxidation by OH preferentially removes ^{12}C, thus leaving behind ethane enriched in ^{13}C, compared to the starting reactant.

3. Methodology

3.1. Experimental Isotopic Measurements During the Ethane Oxidation Reaction

Experiments of ethane oxidation by OH were conducted under atmospheric pressure and at constant temperature (243 K, 253 K, 263 K, 273 K, 288 K, and 303 K). Propane was added to the reaction system as a reference compound to verify the ethane oxidation chemistry. Both ethane and propane isotope ratios were investigated at natural $^{13}C/^{12}C$ abundances. For each examined temperature, the KIE was derived experimentally from the changes in $\delta^{13}C$ and concentration during the course of the reaction, measured by thermal desorption-gas chromatography-combustion-isotope ratio mass spectrometry (TD-GC-C-IRMS).

Ethane and propane oxidation experiments were carried out in a reaction chamber housed in a temperature controlled oven that can accurately achieve and maintain the programmed temperature over long time periods. Details on the used construction are given in the supporting information.

Inside the chamber, OH radicals were generated by the photolysis of hydrogen peroxide, H_2O_2:

(R1) $$H_2O_2 \xrightarrow{h\nu,\lambda=254\ \text{nm}} 2{\bullet}OH$$

To this end, gaseous H_2O_2 was prepared by injecting 2.5 to 10.0 mL of liquid hydrogen peroxide (H_2O_2, 50 wt % in H_2O, Sigma-Aldrich Corporation, USA) into a 6 L Siltek-coated canister (SilcoCan 24182–650, Restek Corporation, USA) under vacuum and subsequently, by pressurizing the canister to 2.5 bars with ultrapure nitrogen.

For the reaction, 150 to 300 μL ethane (C_2H_6, 99.95%, Linde AG, Germany) and 150 μL propane (C_3H_8, 99.95%, Linde AG, Germany) were separately introduced into the reaction chamber using a 150 μL gas loop fixed on a four-port valve. The gases were flushed in by ultrapure nitrogen. After mixing the gases, 9 L of gaseous H_2O_2 was added. The oxidation reactions were initiated by turning the UV lamps on:

(R2) $$C_2H_6 + {\bullet}OH \xrightarrow{k_{\text{ethane}}} H_2O + {\bullet}C_2H_5$$

(R3) $$C_3H_8 + {\bullet}OH \xrightarrow{k_{\text{propane}}} H_2O + {\bullet}C_3H_7$$

where

$$k_{\text{ethane}} = 6.9{\times}10^{-12}\ \exp\left(\frac{-1000{\pm}100}{T}\right)\text{cm}^3\ \text{molecule}^{-1}\ \text{s}^{-1} \tag{5}$$

and

$$k_{\text{propane}} = 7.6{\times}10^{-12}\ \exp\left(\frac{-585{\pm}100}{T}\right)\text{cm}^3\text{molecule}^{-1}\ \text{s}^{-1} \tag{6}$$

are the International Union of Pure and Applied Chemistry (IUPAC) recommended rate coefficients for the reactions (R2) and (R3) [*Atkinson et al.*, 2006].

For each temperature, at least three experiments were conducted. An overview of the experiments, including the volume of ethane and propane introduced into the reactor, the injected H_2O_2 into the canister, the number of UV lamps switched on, the duration, and the number of samples analyzed during each reaction, is given in Table S1 (supporting information).

A 10 mL stainless steel sample loop mounted on a six-port valve was used to transfer gas samples from the reaction chamber to the preconcentration unit of the TD-GC-C-IRMS. The 1/8″ transfer lines were either of Teflon (inside the oven) or of stainless steel (outside the housing). For each experiment, up to 15 gas samples of 10 mL were taken automatically every 90 min from the temperature controlled reaction chamber. After opening the sampling valve, the sample loop was filled with the gas sample at a flow rate of 2 mL min^{-1}. The gas sample flow rate was controlled by a needle valve and a mass flow controller located between the sampling valve and the diaphragm pump. He (99.9999%, AIR LIQUIDE Deutschland GmbH, Germany) was used as the carrier gas to transfer the sample from the sampling loop to the preconcentration unit. The carrier gas flow rate was controlled by an electronic pneumatic control (EPC) unit. All transfer lines, the sample valve, and the sampling loop were maintained at 333 K. The sampling procedure and the EPC unit were controlled by MSD ChemStation E.02.00.493 (Agilent Technologies, USA) software package.

For this work, only two of three cryogenic traps of the custom-built preconcentration unit (thermo desorption system large (TDSL), GERSTEL GmbH & Co. KG, Germany—[*Iannone et al.*, 2008]—were operated. Through alternatively cooling-heating of the cooled injection system (CIS) and the cryogenic trapping system (CTS), an optimal focusing of the reaction gases was achieved prior to the GC separation. Inside the CIS, a Silcotek deactivated quartz inlet liner (L = 71 mm, OD = 3 mm, and ID = 2 mm) was packed with Carbosieve S-III adsorbent (60–80 mesh, Sigma-Aldrich Corporation, USA), giving best performances in trapping light hydrocarbons. The software package TDGL Large V0.5 (GERSTEL GmbH & Co. KG, Germany) was used to control TDSL temperature program and give the start signal for the GC program. The CIS was precooled to 153 K by using liquid nitrogen. After reaching the programmed temperature, the 10 mL sample was transferred from the sample loop to the CIS by using a helium flow of 2.5 mL min^{-1}. The mixture containing ethane and propane was trapped for 10 min and then thermally desorbed at 573 K. The heating rate for the CIS was 1 K s^{-1}. Thus, the mixture was quantitatively transferred to the CTS, precooled at 123 K. Finally, the CTS was abruptly heated to 453 K at a rate of 10 K s^{-1} and the GC separation started.

The GC (6890 G1530A, Agilent Technologies, USA) was equipped with two columns, Rt-Q-BOND (30 m length, 0.32 mm ID (inner diameter), 10 μm film thickness, Restek Corporation, USA) and Rxi-5ms column (30 m length, 0.32 mm ID, 0.25 μm film thickness, Restek Corporation, USA). An EPC maintained a constant flow of helium at 2.5 mL min^{-1}. The GC temperature program started at 243 K, ramped at a rate of 5 K min^{-1} to 423 K, being held there for 4 min. The fractions of GC eluate, containing well-separated peaks of ethane and propane, with retention time of 43 and 57 min, respectively, (see Figure S2, supporting information), were transferred to a mass spectrometer (MSD, 5975C, Agilent Technologies, USA) for chemical identification and to the IRMS (IsoPrime, Micromass Ltd., UK) for concentration and isotope ratio measurements. The rest was sent to a flame ionization detector (Agilent Technologies, USA). The MSD ChemStation software was used to operate the GC program, as well as for chemical identification.

For isotopic measurements, approximately 80% of the total flow was transferred to a combustion interface, which quantitatively oxidized ethane and propane to CO_2 and water [*Merritt et al.*, 1995]. The interface, heated to at 1123 K, consists of a quartz tube packed with 0.1 to 0.5 mm CuO granules. The water was removed by passing the gas stream through a tubular Nafion permeation dryer (0743390, Thermo Fisher Scientific Inc., USA). Following the combustion process, dry CO_2 was introduced to the IRMS to measure *m/z* 44, 45, and 46. For the calibration of the isotope ratio measurements, 15 online open-split 30 s injections of CO_2 working reference gas were done for each chromatogram, alternating with the peaks of interest. The working CO_2 standard used in the measurements was calibrated against VPDB [*Coplen*, 1994]. The software package MassLynx Inorganic Build 4.0.0.792 (GV Instruments Ltd., UK) was employed to operate IRMS and to acquire and evaluate the isotopic data. Regular linearity and stability tests together with gas standard measurements were carried out to ensure the isotopic measurement quality. The linearity tests showed that the IRMS worked properly in the range of 0.3 nA to 8.8 nA. Stability tests for the IRMS were carried out by ten CO_2 reference gas injections, each for 30 s. The experiments were initiated only if three consecutive stability tests gave standard deviations of less than 0.1% for the ratios ^{45}R and ^{46}R (the ratios of the peak areas of *m/z* 45 and *m/z* 46 to the peak area of *m/z* 44, respectively).

3.2. Validation Tests

A number of tests were conducted to evaluate the performances of all elements along the instrumental setup, from the temperature controlled reaction chamber to the TD-GC-C-IRMS.

The temperature stability of the oven was characterized at 303, 288, 273, 263, 253, and 243 K. Two thermocouples were introduced at the base and rear side of the reaction chamber, to monitor temperatures at different locations in the oven. The temperatures were recorded manually every minute for a duration of 80 min. The recording started 10 min after switching on the temperature controller. Due to the rotary fan inside the chamber, a constant temperature, consistent with the temperature in the oven, was reached inside the FEP bag after 5 to 15 min. Furthermore, running the UV lamps did not influence the temperature stability of the oven in the investigated temperature range. Overall, the oven exhibited a stability of better than ±300 mK for the investigated range. The measured temperatures were 303.0 ± 0.1, 288.0 ± 0.2, 272.7 ± 0.3, 262.9 ± 0.3, 253.2 ± 0.3, and 242.7 ± 0.3 K with relative standard deviations of up to 0.12%. Average temperature, uncertainties, and maximum deviations within the reaction chamber can be found in Table S2 in the supporting information.

Moreover, at each set temperature, the accuracy and reproducibility of the method were tested using ethane/propane mixtures with known composition and isotope ratios. Prior to each experiment, the reaction chamber was cleaned by pumping out the air from inside. The oven was heated to 313 K. Ultrapure nitrogen (N2, 99.9999%, Linde AG, Germany) was filled into the chamber, kept for 30 min, and then flushed out. The procedure was repeated three times. A blank concentration measurement was carried out, to test the cleanliness of the bag. To carry out the concentration and $\delta^{13}C$ stability tests, the experimental procedure previously described was employed. The only difference to the KIE experiments was that there was no oxidation reaction taking place in the reaction chamber. Ethane and propane were injected in the bag. Instead of gaseous H_2O_2, the same volume of pure N_2 was added. The UV lamps were off. All concentration and $\delta^{13}C$ stability experiments were conducted for 17 h, reproducing twelve GC-IRMS measurements of 90 min each. The first measurement started 30 min after reaching the required temperature in the reaction chamber. Neither a systematic change of ethane or propane concentrations nor a change in relative concentration of ethane compared to propane was observed, indicating that the reaction chamber was free of leaks and that there were no other loss processes of the compounds of interest along the transfer lines or in the TD-GC-C-IRMS system. Tests with different injected ethane amounts—from 150 ppb up to 1000 ppb—showed a reproducible $\delta^{13}C$ value within the error ranges, being -32.60 ± 0.37. This implies that different ethane amounts adsorbed in the CIS do not introduce any significant isotopic fractionation. Overall, the instrumental and methodological performances of the sampling and TD-GC-C-IRMS systems were highly reproducible. The averaged concentration changes, represented as ratios $([C]_t/[C]_0) \times 100\%$, and $\delta^{13}C$ of ethane and propane during the stability experiments carried out at as well as the corresponding average and errors can be found in Table S3 in the supporting information.

The OH oxidation chemistry during the KIE experiments was tested by the relative rate method, commonly associated with highly reactive radical reactions. Since OH measurements are not feasible in the above described setup, direct determination of k_{ethane} is not possible. Instead, the concentration of the ethane/propane pair during each single experiment was simultaneously monitored. In the absence of other loss processes, the ratio of the respective OH rate coefficients depends on the ratio of the consumption of the pair of tracers [*Finlayson-Pitts and Pitts*, 1986]:

$$R_{\mathrm{ethane/propane}} = \frac{k_{\mathrm{ethane}}}{k_{\mathrm{propane}}} = \frac{\ln\left([\mathrm{ethane}]_0/[\mathrm{ethane}]_t\right)}{\ln\left([\mathrm{propane}]_0/[\mathrm{propane}]_t\right)} \tag{7}$$

where $[\mathrm{ethane}]_0$, $[\mathrm{ethane}]_t$, $[\mathrm{propane}]_0$, and $[\mathrm{propane}]_t$ are the initial concentrations of ethane and propane and at reaction time t. Thus, the actual rate coefficient of the ethane oxidation is derived as follows:

$$k_{\mathrm{ethane}} = R_{\mathrm{ethane/propane}}\, k_{\mathrm{propane}}. \tag{8}$$

3.3. Kinetic Models for Theoretical KIE Calculations

Chemical quantum mechanics and kinetics calculations were carried out for the oxidation reactions involving $^{12}CH_3{}^{12}CH_3$ or $^{12}CH_3{}^{13}CH_3$ to calculate the absolute rate coefficients k_{12} and k_{13}, respectively. The KIE was determined as the ratio k_{12}/k_{13}. Note that the symmetry number of ^{13}C-ethane is half of that for

^{12}C-ethane. Also, two distinguishable transition states exist, with the H abstraction occurring either from the ^{12}C or ^{13}C atom:

(R4) $$^{12}CH_3{}^{13}CH_3 + \bullet OH \longrightarrow H_2O + \bullet{}^{12}CH_2{}^{13}CH_3$$

(R5) $$^{12}CH_3{}^{13}CH_3 + \bullet OH \longrightarrow H_2O + \bullet{}^{13}CH_2{}^{12}CH_3.$$

The reactions were assumed to be in the high-pressure regime and a temperature range from 150 to 400 K was considered.

The methodology for calculating rate coefficients is described in detail in the supporting information. Quantum mechanics was employed to calculate the electronic properties of stationary points along the reaction pathway at various levels of theory [*Alecu et al*., 2010; *Bao et al*., 2017; *Barone et al*., 2010; *Becke*, 1988, 1993; *Dunning*, 1989; *Kendall et al*., 1992; *Lee et al*., 1988; *Malick et al*., 1998; *Pople et al*., 1987; *Purvis and Bartlett*, 1982; *Zhao and Truhlar*, 2008]; The optimized geometries at M06-2X/aug-cc-pVTZ (99,974 grid) level of theory were chosen for this study. Energy refinements were carried out at CCSD(T)/aug-Schwartz(DTQ) level of theory on the M06-2X optimized structures [*Martin and Taylor*, 1997]. All quantum chemical calculations were performed using the Gaussian-09 software suite [*Frisch et al*., 2010]. Transition state theory was applied to evaluate rate coefficients, using the quantum mechanics calculated properties [*Barker*, 2001; *Barker et al*., 2012, 2016; *Basire et al*., 2008; *Eckart*, 1930; *Fernández-Ramos et al*., 2006; *Hernandez and Miller*, 1993; *Johnston and Heicklen*, 1962; *Kilpatrick and Pitzer*, 1949; *Meyer*, 1970; *Miller et al*., 1990; *Nguyen and Barker*, 2010; *Nguyen et al*., 2010; *Senosiain et al*., 2001; *Vereecken et al*., 2015; *Wagner*, 2013]. Due to the limited amount of available computational resources and software, we identified a limited set of technique combinations creating six theoretical kinetic models.

Model A includes a canonical transition state theory (CTST) analysis using our in-house software. Here the molecular rotation is treated classically with the TS as an asymmetric top. All internal modes are described as harmonic oscillators, using M06-2X/aug-cc-pVTZ (99,974 grid) rovibrational data, where the wave numbers and zero point vibrational energy (ZPE) are scaled by 0.971. Asymmetric Eckart tunneling is implemented using the scaled M06-2X imaginary wave number.

Model B is similar to Model A but uses zero-curvature tunneling (ZCT) with M06-2X IRC energy profiles.

Within *Model C*, the CTST analysis is done by the MultiWell software [*Barker*, 2001, 2009; *Barker et al*., 2016]. Compared to Model A, the following modifications are implemented: (i) the molecular rotation is treated as a quantum rotor; the transition state is approximated as a symmetric top using arithmetic averaging of the two similar asymmetric top rotational constants; (ii) the unscaled harmonic vibrational wave numbers are used throughout the calculations of the partition functions, of the asymmetric Eckart tunneling, as well as for the ZPE corrections.

Model D carries out a CTST analysis similarly to Model C but replaces internal rotation modes by quantized one-dimensional internal rotors.

Within *Model E*, a semiclassical transition state theory (SCTST) analysis is implemented with the MultiWell software [*Hernandez and Miller*, 1993; *Miller*, 1975, 1977; *Miller et al*., 1990; *Nguyen et al*., 2010, 2011]. M06-2X/aug-cc-pVTZ (99,974 grid) anharmonic rovibrational data and unscaled wave numbers and anharmonicities $\chi_{i,j}$ are used. The vibrational modes corresponding to internal rotation are replaced by one-dimensional separable rotors. The $\chi_{i,j}$ values pertaining to the two OH wagging modes are set to zero, avoiding inconsistent anharmonicity treatment. Multidimensional tunneling is implicitly used in the SCTST. The ZPE corrections reflect the zeroing of χ values, and the lowest energy level of the internal rotors, except that the χ_0 value, is used unmodified.

Model F approximates a harmonic model with multidimensional tunneling. It is similar to Model E, except that all modes are treated as harmonic oscillations and all $\chi_{i,j}$ values are set to zero. The ZPE corrections are based on a harmonic oscillator model.

As discussed in the supporting information, Models E and F suffer from numerical and methodological problems, even though they may appear at first glance as reasonable implementations that attempt the best result for an imperfect data set. The predicted absolute rate coefficients, KIE values, and their temperature dependence carry a large uncertainty.

4. Results and Discussions

4.1. Experimental Rate Coefficients for the Ethane Reaction With OH

From the relative decay of the ethane/propane tracer pair in the course of the reaction, the ratio of the OH rate coefficients $R_{ethane/propane}$ was determined. As shown in equation (7), this is given by the slope of the line fitted to the experimental data plotted as $\ln([ethane]_0/[ethane]_t)$ against $\ln([propane]_0/[propane]_t)$. Subsequently, the actual k_{ethane} was derived within the temperature range of interest according to equation (8) and using the IUPAC recommended $k_{propane}$ temperature dependence (equation (6)). The statistical errors reported in this work are calculated by propagating the uncertainties through all steps of the calculations.

At 303 K, the ratio was found to be 0.235 ± 0.016 (Figure 1). By employing the IUPAC recommended $k_{propane}$ value of 11.02 ± 0.43 × 10^{-13} cm^3 $molecule^{-1}$ s^{-1} (see equation (6) for T = 303 K), k_{ethane} of 2.59 ± 0.73 × 10^{-13} cm^3 $molecule^{-1}$ s^{-1} was derived.

Similarly, k_{ethane} was determined at each examined temperature (see Figure S2 in the supporting information). These experimentally determined rate coefficients are presented in Table 1 together with the values recommended by the IUPAC Subcommittee on Gas Kinetic Data Evaluation for Atmospheric Chemistry [*Atkinson et al*., 2006]. The latter were derived from equation (5) by using T = 303, 288, 273, 263, 253, and 243 K.

Figure 2 depicts a summary of the here derived absolute k_{ethane} values, in addition to those hitherto reported in the temperature range 180–400 K. The IUPAC recommended temperature dependence of the rate coefficients for the ethane reaction with OH is also presented. Overall, it is shown that the k_{ethane} values obtained experimentally in this study and their temperature dependence show good agreement with the available literature data within the error ranges.

4.2. Experimental KIE

For each individual oxidation experiment carried out at a constant temperature, the ethane and propane $\delta^{13}C$ values were measured in the course of the reaction. Compared to the start of the reaction, the samples showed a ^{13}C enrichment of up to 26‰ for ethane and 12‰ for propane, when 95% of the reactant was consumed (Figure 3). This behavior was observed during all experiments, showing a steeper $\delta^{13}C$ increase at reaction conversion higher than 80%.

From the temporal evolution of concentrations and $\delta^{13}C$ values during the reaction, the KIE of the oxidation reactions was determined. At 303 K, the slopes of the line fitted to the experimental data plotted as $\ln([^{12}C]_t/[^{12}C]_0)$ against $\ln([\delta^{13}C_t + 1000]/[\delta^{13}C_0 + 1000])$ were found to be −136.39 ± 7.35 for ethane and −261.64 ± 9.31 for propane (Figure 4). These values correspond to KIE/(1-KIE) (see equation (4)), translating in ε values of 7.39 ± 0.40 and 3.84 ± 0.14‰, respectively.

Similarly, the KIE for the ethane and propane oxidation was determined at each examined temperature (Figure S3 in the supporting information). The ε values from this work are summarized in Table 2 together with previously reported ones [*Anderson et al*., 2004; *Rudolph et al*., 2000].

The KIE temperature dependence is illustrated in Figure 5. The ε values of ethane from this study at 303.0 ± 0.1 and 288.0 ± 0.2 K were found to be 7.16 ± 0.54 and 7.45 ± 0.48‰, respectively. Within the error ranges, they show good agreement with the value reported by *Anderson et al*. [2004], i.e., 8.57 ± 1.95‰ at 296 ± 4 K. At 303.0 ± 0.1 K, the propane KIE value was determined to be 3.61 ± 0.37‰, well agreeing with the earlier literature value of 3.44 ± 0.26‰ [*Rudolph et al*., 2000] and being very different from the value of 5.46 ± 0.35‰ reported by *Anderson et al*. [2004]. On the other side, both KIE values of ethane and propane obtained in this work are also in fairly good agreement with the values predicted using the inverse dependence on carbon number [*Rudolph et al*., 2000], being 8.3 and 5.5‰, respectively.

It should be noted that the KIE experiments carried out near room temperature proved a considerable improvement of the measurement precision, compared to previous works. Also at lower temperatures, the observed error ranges were very narrow, showing standard deviations between 0.15‰ and 2.19‰. The ε measurements at 242.7 ± 0.3 K were associated with a higher standard deviation of the mean, i.e., 9.42 ± 2.19‰. Two aspects might be responsible for it. First, at 243 K the ethane reacts with OH 2.3 times

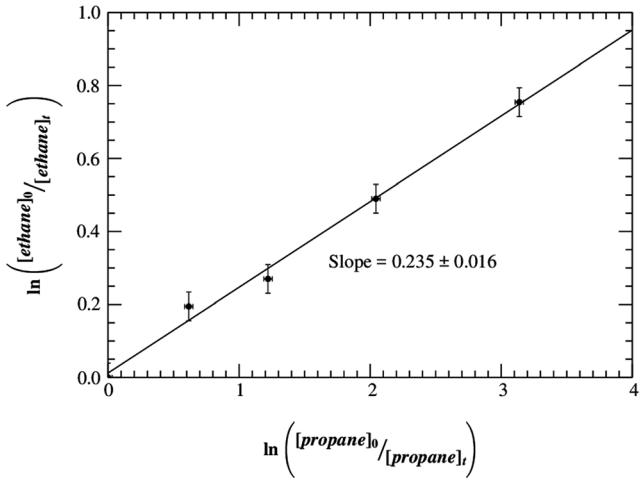

Figure 1. Natural logarithms of the ethane and propane concentrations relative to initial concentration (black full circles) during the oxidation reaction by OH at 303.0 ± 0.1 K (Experiment No. 2, Table S1 in the supporting information), as well as the weighted linear least squares fit to the experimental data (black line).

slower than at 303 K. Second, due to the very low H_2O_2 vapor pressure, the OH production is strongly hindered at this temperature, thus significantly reducing the oxidation reaction rate. Both combined lead to a significantly lower conversion for the optimal experiment maximum duration. The experiments showed that carrying out experimental KIE studies at temperatures lower than 243 K with the presented instrumentation is prone to high uncertainties; therefore, other solutions to investigate the temperature dependence are required.

Compared to ethane, lower accuracy was expected when deriving the KIE of propane oxidation by OH across the whole temperature range. Since all experiments were optimized to cover the entire dynamical range of the ethane + OH reaction, the propane was completely consumed long before the proposed conversions of the ethane oxidation have been reached. Therefore, few data points for the propane concentration and $\delta^{13}C$ were measured during each experiment, most of them belonging to the high side of the conversion range. This study demonstrates that concurrent determination of accurate KIE values for two compounds with rate coefficients differing by a factor of 6 is highly challenging. Further experiments are necessary, with optimized configurations to ensure precise determination of the propane oxidation KIE and its temperature dependence. Nevertheless, it was shown that propane was a good reference compound for experimentally deriving kinetic information for the reaction ethane + OH.

Overall, this experimental study showed a slight increasing trend of the KIE of ethane + OH toward low temperatures, adding up to approximately 0.4 ± 0.1‰ per 10 K. This change is likely to be more pronounced at temperatures lower than 263 K. The temperature dependence of propane KIE is inconclusive.

4.3. Theoretical Rate Coefficient Predictions

The results of the theoretical calculations using the six different kinetic models are shown in Figure 6. We compared the temperature dependence of the rate coefficients for the reaction $^{12}CH_3{}^{12}CH_3$ + OH from our present work with the modified Arrhenius fit recommended by IUPAC [*Atkinson et al.*, 2006]. It is shown that the CTST Models A and C, which implement a harmonic oscillator rigid rotor, yield similar results. They closely reproduce the absolute rate coefficient within a factor of 1.4 at the lowest examined temperature, yet showing a slightly steeper temperature dependence than that expressed by IUPAC. The wave number scaling, the

Table 1. Summary of the Rate Coefficients (k_{ethane}, cm^3 $molecule^{-1}$ s^{-1}), for the Ethane Oxidation by OH, Determined by Using the Relative Rate Method (for Details See Text), As Well As the Recommended IUPAC Values [*Atkinson et al.*, 2006], Calculated From Equation (5) by Using T = 303, 288, 273, 263, 253, and 243 K

	k_{ethane}, 10^{-13} cm^3 $Molecule^{-1}$ s^{-1}	
T, K	This Work	IUPAC [*Atkinson et al.*, 2006]
303.0 ± 0.1	2.55 ± 0.73	2.54 ± 0.99
288.0 ± 0.2	2.28 ± 0.67	2.14 ± 0.89
272.7 ± 0.3	1.56 ± 0.49	1.77 ± 0.78
262.9 ± 0.3	1.54 ± 0.53	1.54 ± 0.71
253.2 ± 0.3	1.66 ± 0.66	1.33 ± 0.64
242.7 ± 0.3	1.34 ± 0.66	1.13 ± 0.57

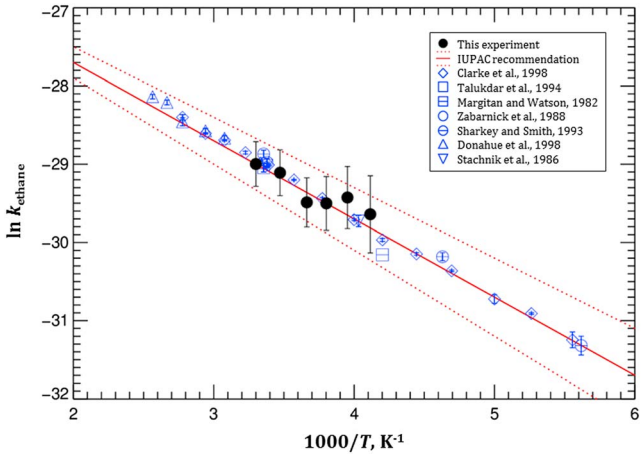

Figure 2. Experimentally determined rate coefficients (k_{ethane}, cm^3 $molecule^{-1}$ s^{-1}) for the ethane oxidation by OH at 303.0 ± 0.1, 288.0 ± 0.2, 272.7 ± 0.3, 262.9 ± 0.3, 253.2 ± 0.3, and 242.7 ± 0.3 K from this work and available data from the literature [*Clarke et al*., 1998; *Donahue et al*., 1998; *Margitan and Watson*, 1982; *Sharkey and Smith*, 1993; *Stachnik et al*., 1986; *Talukdar et al*., 1994; *Zabarnick et al*., 1988] as well as the temperature dependence of the k_{ethane} recommended by the IUPAC Subcommittee on Gas Kinetic Data Evaluation for Atmospheric Chemistry [*Atkinson et al*., 2006] and its uncertainty ranges.

use of quantized versus classical molecular rotors, their symmetrizing, and the use of different software packages had only a negligible influence on the predictions, such that the A and C model results vary by less than 10%. The only significant differences can be seen in the low-temperature range caused by different ZPE corrections. Replacing the Eckart tunneling by the ZCT tunneling (Model B) increased the rate coefficient by about a factor of 2 throughout the examined temperature range but kept a similar temperature dependence. The SCTST Model F, which mimics a harmonic model but with multidimensional tunneling, yielded absolute rate coefficients very close to the experimental data, showing a somewhat stronger temperature dependence and curvature in the Arrhenius plot, which suggests that tunneling was overestimated within this simulation.

The changes made in Model D by explicitly considering the internal rotation lead to a temperature dependence of $k(T)$ very close to the IUPAC recommendation, but the absolute values are exceeded by a factor of 2. The increased absolute rate coefficients relatively to Model C are due to the changes in ZPE corrections, where the smaller ZPE of the internal rotors lowered the effective reaction barrier. Increasing the barrier height by ~0.4 kcal mol^{-1} brings the predictions in excellent agreement with the IUPAC data; such a change

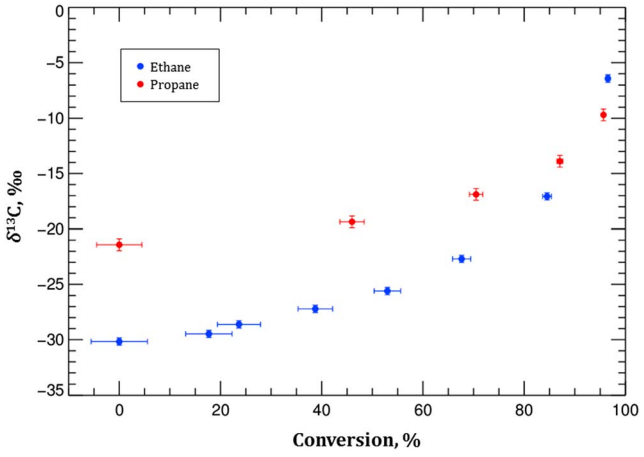

Figure 3. $\delta^{13}C$ values observed during the oxidation reactions of ethane and propane by OH, carried out at 303.0 ± 0.1 K (Experiment number 2, Table S1 in the supporting information).

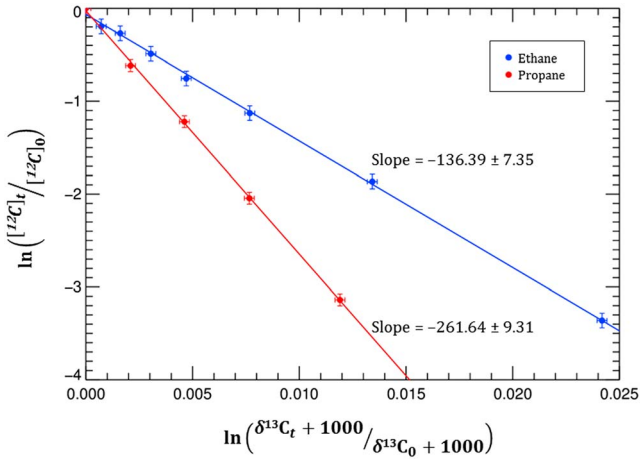

Figure 4. Experimental KIE determination for the OH oxidation reaction of ethane and propane at 303.0 ± 0.1 K (Experiment number 2, Table S1 in the supporting information, for detail, see text).

is within the quantum chemical calculation uncertainties and could emerge from higher-level calculations as applied to smaller systems [*Barker et al*., 2012].

The absolute rate coefficient predictions using Model E exceed the IUPAC values by several orders of magnitude. This is because there is a strong decrease in the ZPE-corrected energy barrier, which in turn is linked to the large errors on the anharmonicity constants. As for Model F, the tunneling corrections seem to have been overestimated, leading to a more strongly curved Arrhenius plot that noticeably deviates from the other results.

4.4. Theoretical KIE

Based on the above described theoretical kinetic models, k_{12} and k_{13} and their ratio were calculated. The derived ε values (equations (2) and (3)) are presented in Figure 7. Note that our toolset is not yet optimized for propagating the very small differences between the ^{12}C and ^{13}C calculations across the different steps, leading to some KIE numerical noise (see Figure 7). Both KIE from Models A and C, i.e., the harmonic CTST with Eckart tunneling, show no temperature dependence for the most part of the examined range. Despite the small differences in the absolute $k(T)$ derived from these two models, the corresponding KIEs differ by a factor of 1.5. Model B, which differs by using ZCT tunneling, shows a stronger negative temperature dependence for the KIE at the lowest temperatures but remains comparable to Models A and C. Model D, which explicitly treats the internal rotation, predicts a higher KIE than Model C, additionally showing a slight negative temperature dependence. While the obtained KIE trend is in all cases comparable to the experimental one, it is clear that the theoretical prediction of the KIE values is unprecise. As these three kinetic models are rather

Table 2. Experimental KIE for the Oxidation Reactions of Ethane and Propane by OH in the Temperature Range of 243 K to 303 K, Together With Available Published Data [*Anderson et al*., 2004; *Rudolph et al*., 2000]

	ε, ‰	
T, *K*	Ethane	Propane
	This Work	
303.0 ± 0.1	7.16 ± 0.54	3.65 ± 0.36
288.0 ± 0.2	7.45 ± 0.48	3.60 ± 0.31
272.7 ± 0.3	7.36 ± 0.28	3.66 ± 0.15
262.9 ± 0.3	7.61 ± 0.28	3.61 ± 0.34
253.2 ± 0.3	8.89 ± 0.90	4.87 ± 0.56
242.7 ± 0.3	9.42 ± 2.19	4.31 ± 0.70
	Literature	
296 ± 4 [*Anderson et al*., 2004]	8.57 ± 1.95	5.46 ± 0.35
305 ± 3 [*Rudolph et al*., 2000]	-	3.44 ± 0.26

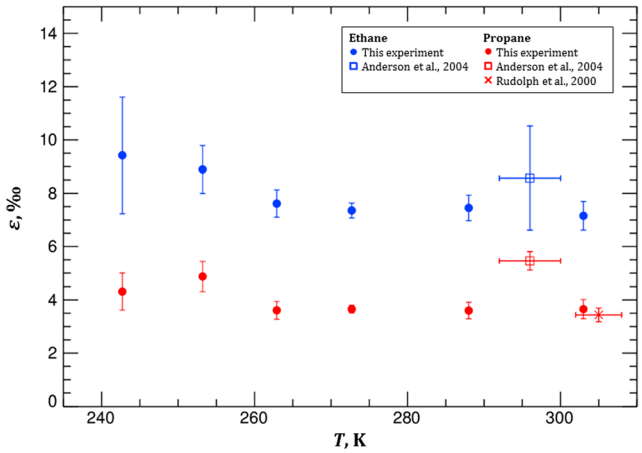

Figure 5. Overview of experimental KIE (ε values,‰) for the oxidation reactions of ethane and propane by OH from this work, as well as near-room-temperature literature values [*Anderson et al.*, 2004; *Rudolph et al.*, 2000].

comparable, an a priori selection which is the best would be impossible without the benefit of experimental data. Some of the differences may be due to numerical errors propagating through the calculations procedure, as well as numerical artifacts. In addition, the underlying quantum chemical data may not be perfect, which may lead to different cancelation of errors across the different models. Currently, there is no tractable way to eliminate these uncertainties. The comparison with the experimental data suggests that the intrinsic reliability of the KIE predictions is currently not better than a factor of 2.

Figure 7 also shows the KIE derived from the SCTST Model F. These predictions are neither comparable to the experimentally obtained absolute values nor do they show a similar temperature dependence. The ε values derived from Model E are not included in Figure 7, since they are greater than 100‰ KIE and thus fully incompatible with the experimental data. We believe that the failure of Models E and F to predict KIE, despite good performances in calculating $k(T)$, is not the result of the use of the SCTST methodology. Previous studies delivered already fairly good results for smaller systems, i.e., Cl + CH_4 reaction yielding a 2% error for the ab initio $^{12}C/^{13}C$ KIE [*Barker et al.*, 2012]. We rather surmise that the fault is in the use of VPT2 anharmonic vibrational analysis [*Barone et al.*, 2010] for molecules that contain complex degrees of freedom (see supporting information) together with the pitfalls of ad hoc modifications of the obtained data to fit a particular view on the reaction dynamics for ethane + OH.

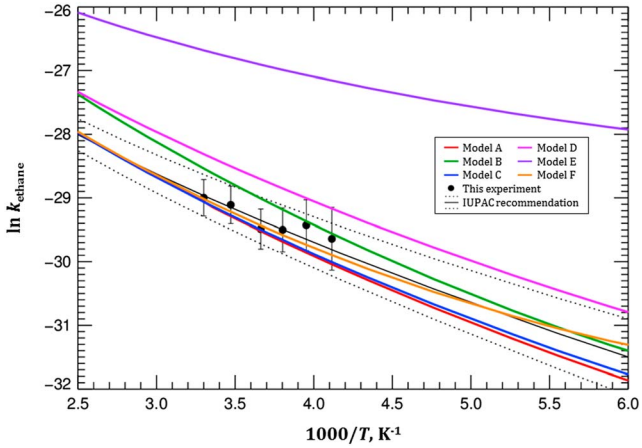

Figure 6. Arrhenius plot of the thermal rate coefficients ($k(T)$, cm^3 $molecule^{-1}$ s^{-1}) for the reaction C_2H_6 + •OH → •C_2H_5 + H_2O involving only ^{12}C calculated by various theoretical kinetic models: Models A–F (for details see text). The experimental values from this work (see section 3.1), and the IUPAC recommended $k(T)$ with its uncertainties are also shown.

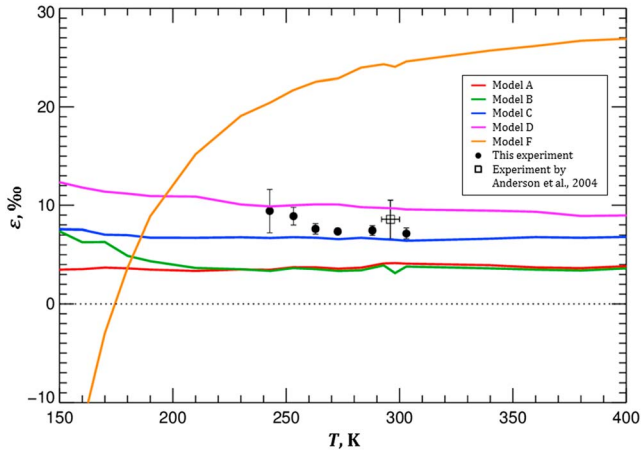

Figure 7. Calculated KIE values (ε, ‰) for the reaction C_2H_6 + •OH → •C_2H_5 + H_2O by various theoretical kinetic models: Models A–D and F comparing with experimental KIE values from this work (see section 3.2) and literature values at room temperature [*Anderson et al*., 2004].

To the best of our knowledge, the reaction C_2H_6 + OH → C_2H_5 + H_2O is the biggest chemical system that has been theoretically investigated for stable carbon KIE predictions using absolute rate coefficient calculations. Limitations in computing resources restricted the level of the implemented theory for the KIE prediction. Nevertheless, this study opened the possibility for comparisons among different approaches. Additionally, it gives information in which direction the higher levels of theory should be implemented in further calculations, regarding geometry optimizations, anharmonicity frequencies, tunneling effect, and internal rotation.

5. Conclusions

Laboratory experiments to determine the KIE temperature dependence of the ethane oxidation by OH radicals were carried out at ambient pressure. The examined temperature range was from 243 K to 303 K. Propane was used as a reference compound to verify the ethane chemistry. The reactants were investigated at natural isotope abundance in a temperature controlled reaction chamber. Isotope ratios of the gas phase components during the course of the reactions were measured. The method was adjusted to optimize the dynamical range of the ethane KIE with OH, which was derived at each examined temperature from the temporal evolution of the ethane $\delta^{13}C$ and concentration. At 303 ± 0.1 and 288.0 ± 0.3 K, the KIE values for the ethane oxidation by OH were found to be 7.16 ± 0.54 and 7.45 ± 0.48‰, respectively, showing a noticeable improvement of the measurement precision compared to the only available KIE value of 8.57 ± 1.95‰ at 296 ± 4 K reported by *Anderson et al*. [2004]. Over the investigated temperature range, a slight increasing tendency of KIE toward lower temperatures was found, being approximately 0.4 ± 0.1‰ per 10 K. Though within the error ranges, the temperature dependence is inconclusive.

Quantum chemical calculations together with transition state theory were employed to theoretically determine the temperature dependence of KIE in the temperature range of 150 K to 400 K. The goal of this study was to better understand the reaction kinetic, as well as to investigate KIE at temperatures, where the experimental work has strong limitations. The quantum mechanical calculations were performed employing the CCSD(T)/CBS//M06-2X/aug-cc-pVTZ quantum chemical method, combined with canonical transition state theory (CTST) and semiclassical transition state theory (SCTST) in chemical kinetics calculation. Tunneling effect and internal rotation treatments were also included in the calculations. The theoretically computed KIE values using CTST models combining the above mentioned methods showed similar trends with the experimental data yet differed roughly by a factor of 2. Two models implementing SCTST yielded results very different from observations. Nevertheless, the theoretical calculations delivered valuable conclusions toward a better understanding of the reaction kinetics.

Overall, this work delivered a substantial basis for future investigations on the global distribution of tropospheric ethane sources and sinks by using the ^{13}C isotopic composition. The refined KIE at room

temperature is about 1.5‰ lower than the hitherto reported value. Its implementation in a global chemical transport model is anticipated to result in a better agreement between the model estimated and the observed ethane $\delta^{13}C$. Improved theoretical calculations will also provide the KIE at low atmospheric temperatures, which cannot be experimentally determined. This might allow fine structures to be resolved in regions where air masses alter at very low temperatures.

Acknowledgments
We gratefully acknowledge Jochen Rudolph, at the Centre for Atmospheric Chemistry, York University, for sharing his expertise with regard to kinetic isotope effects during VOC atmospheric degradation reactions. In accordance with AGU data policy, further descriptions of methodology and results can be found in the supporting information.

References

Alecu, I. M., J. Zheng, Y. Zhao, and D. G. Truhlar (2010), Computational thermochemistry: Scale factor databases and scale factors for vibrational frequencies obtained from electronic model chemistries, *J. Chem. Theory Comput.*, *6*(9), 2872–2887.

Anderson, R. S., L. Huang, R. Iannone, A. E. Thompson, and J. Rudolph (2004), Carbon kinetic isotope effects in the gas phase reactions of light alkanes and Ethene with the OH radical at 296 ± 4 K, *J. Phys. Chem. A*, *108*, 11,537–11,544.

Atkinson, R., D. L. Baulch, R. A. Cox, J. N. Crowley, R. F. Hampson, R. G. Hynes, M. E. Jenkin, M. J. Rossi, J. Troe, and I. Subcommittee (2006), Evaluated kinetic and photochemical data for atmospheric chemistry: Volume II—Gas phase reactions of organic species, *Atmos. Chem. Phys.*, *6*(11), 3625–4055.

Finlayson-Pitts, B., and J. N. Pitts Jr. (1986), Fundamentals and experimental techniques, in *Atmospheric Chemistry*, pp. 1244–1244, Wiley-VCH Verlag GmbH & Co. KGaA, Weinheim.

Bao, J. L., J. Zheng, I. M. Alecu, B. J. Lynch, Y. Zhao, and D. G. Truhlar (2017), Database of frequency scale factors for electronic model chemistries, Version 3 Beta 2. [Available at https://comp.chem.umn.edu/freqscale/version3b2.htm.]

Barker, J. R. (2001), Multiple-well, multiple-path unimolecular reaction systems. I. MultiWell computer program suite, *Int. J. Chem. Kinet.*, *33*(4), 232–245.

Barker, J. R. (2009), Energy transfer in master equation simulations: A new approach, *Int. J. Chem. Kinet.*, *41*(12), 748–763.

Barker, J. R., T. L. Nguyen, and J. F. Stanton (2012), Kinetic isotope effects for Cl + CH4 ⇌ HCl + CH3 calculated using ab initio semiclassical transition state theory, *Chem. – Eur. J.*, *116*(24), 6408–6419.

Barker, J. R. N., et al. (2016), *MultiWell-2016 Software Suite*, Univ. of Michigan, Ann Arbor, Mich.

Barone, V., J. Bloino, C. A. Guido, and F. Lipparini (2010), A fully automated implementation of VPT2 infrared intensities, *Chem. Phys. Lett.*, *496*(1–3), 157–161.

Basire, M., P. Parneix, and F. Calvo (2008), Quantum anharmonic densities of states using the Wang-Landau method, *J. Chem. Phys.*, *129*(8), 081101.

Becke, A. D. (1988), Density-functional exchange-energy approximation with correct asymptotic behavior, *Phys. Rev. A*, *38*(6), 3098–3100.

Becke, A. D. (1993), A new mixing of Hartree–Fock and local density functional theories, *J. Chem. Phys.*, *98*(2), 1372–1377.

Brand, W. A., S. S. Assonov, and T. B. Coplen (2010), Correction for the 17O interference in $\delta(^{13}C)$ measurements when analyzing CO_2 with stable isotope mass spectrometry (IUPAC technical report), *Pure Appl. Chem.*, *82*(8), 1719–1733.

Clarke, J. S., J. H. Kroll, N. M. Donahue, and J. G. Anderson (1998), Testing frontier orbital control: Kinetics of OH with ethane, propane, and cyclopropane from 180 to 360 K, *Chem. – Eur. J.*, *102*(48), 9847–9857.

Coplen, T. B. (1994), Reporting of stable hydrogen, carbon, and oxygen isotopic abundances (Technical Report), *Pure Appl. Chem.*, *66*(2), 273–276, doi:10.1351/pac199466020273.

Donahue, N. M., J. G. Anderson, and K. L. Demerjian (1998), New rate constants for ten OH alkane reactions from 300 to 400 K: An assessment of accuracy, *Chem. – Eur. J.*, *102*(18), 3121–3126.

Dunning, T. H. (1989), Gaussian basis sets for use in correlated molecular calculations. I. The atoms boron through neon and hydrogen, *J. Chem. Phys.*, *90*(2), 1007–1023.

Eckart, C. (1930), The penetration of a potential barrier by electrons, *Phys. Rev.*, *35*(11), 1303–1309.

Etiope, G., and P. Ciccioli (2009), Earth's degassing: A missing ethane and propane source, *Science*, *323*(5913), 478.

Fast, P. L., J. C. Corchado, and D. G. Truhlar (1998), *J. Chem. Phys.*, *109*, 6237.

Fernández-Ramos, A., J. A. Miller, S. J. Klippenstein, and D. G. Truhlar (2006), Modeling the kinetics of bimolecular reactions, *Chem. Rev.*, *106*(11), 4518–4584.

Frisch, M. J., et al. (2010), *Gaussian 09*, Gaussian, Inc., Wallingford, Conn.

Gensch, I., A. Kiendler-Scharr, and J. Rudolph (2014), Isotope ratio studies of atmospheric organic compounds: Principles, methods, applications and potential, *Int. J. Mass Spectrom.*, *365–366*, 206–221.

Goldstein, A. H., and S. L. Shaw (2003), Isotopes of volatile organic compounds: An emerging approach for studying atmospheric budgets and chemistry, *Chem. Rev.*, *103*(12), 5025–5048.

Gonzalez-Lafont, A., J. Villa, J. M. Lluch, J. Bertran, R. Steckler, and D. G. Truhlar (1998), Variational transition state theory and tunneling calculations with reorientation of the generalized transition states for methyl cation transfer, *J. Phys. Chem. A*, *102*(19), 3420–3428, doi:10.1021/jp9807672.

Gupta, M. L., R. J. Cicerone, D. R. Blake, F. S. Rowland, and I. S. A. Isaksen (1998), Global atmospheric distributions and source strengths of light hydrocarbons and tetrachloroethene, *J. Geophys. Res.*, *103*(D21), 28,219–28,235, doi:10.1029/98JD02645.

Hernandez, R., and W. H. Miller (1993), Semiclassical transition state theory. A new perspective, *Chem. Phys. Lett.*, *214*(2), 129–136.

Iannone, R., R. Koppmann, and J. Rudolph (2008), The stable-carbon kinetic isotope effects of the reactions of isoprene, methacrolein, and methyl vinyl ketone with ozone in the gas phase, *Atmos. Environ.*, *42*, 8728–8737.

Jenden, P. D., and I. R. Kaplan (1986), Comparison of microbial gases from the middle America trench and Scripps submarine canyon: Implications for the origin of natural gas, *Appl. Geochem.*, *1*(6), 631–646.

Johnston, H. S., and J. Heicklen (1962), Tunnelling corrections for unsymmetrical Eckart potential energy barriers, *J. Phys. Chem.*, *66*(3), 532–533.

Kendall, R. A., T. H. Dunning, and R. J. Harrison (1992), Electron affinities of the first-row atoms revisited. Systematic basis sets and wave functions, *J. Chem. Phys.*, *96*(9), 6796–6806.

Kilpatrick, J. E., and K. S. Pitzer (1949), Energy levels and thermodynamic functions for molecules with internal rotation. III. Compound rotation, *J. Chem. Phys.*, *17*(11), 1064–1075.

Lee, C., W. Yang, and R. G. Parr (1988), Development of the Colle-Salvetti correlation-energy formula into a functional of the electron density, *Phys. Rev. B*, *37*(2), 785–789.

Lin, H., Y. Zhao, B. A. Ellingson, J. Pu, and D. G. Truhlar (2005), Temperature dependence of carbon-13 kinetic isotope effects of importance to global climate change, *J. Am. Chem. Soc.*, *127*(9), 2830–2831.

Malick, D. K., G. A. Petersson, and J. A. Montgomery Jr. (1998), Transition states for chemical reactions I. Geometry and classical barrier height, *J. Chem. Phys.*, *108*(14), 5704–5713.
Margitan, J. J., and R. T. Watson (1982), Kinetics of the reaction of hydroxyl radicals with nitric acid, *J. Phys. Chem.*, *86*(19), 3819–3824.
Martin, J. M. L., and P. R. Taylor (1997), Benchmark quality total atomization energies of small polyatomic molecules, *J. Chem. Phys.*, *106*(20), 8620–8623.
Merritt, D. A., K. H. Freeman, M. P. Ricci, S. A. Studley, and J. M. Hayes (1995), Performance and optimization of a combustion Interface for isotope ratio monitoring gas chromatography/mass spectrometry, *Anal. Chem.*, *67*(14), 2461–2473.
Meyer, R. (1970), Trigonometric interpolation method for one-dimensional quantum-mechanical problems, *J. Chem. Phys.*, *52*(4), 2053–2059.
Miller, W. H. (1975), Semiclassical limit of quantum mechanical transition state theory for nonseparable systems, *J. Chem. Phys.*, *62*(5), 1899–1906.
Miller, W. H. (1977), Semi-classical theory for non-separable systems: Construction of "good" action-angle variables for reaction rate constants, *Faraday Discuss. Chem. Soc.*, *62*, 40–46.
Miller, W. H., R. Hernandez, N. C. Handy, D. Jayatilaka, and A. Willetts (1990), Ab initio calculation of anharmonic constants for a transition state, with application to semiclassical transition state tunneling probabilities, *Chem. Phys. Lett.*, *172*(1), 62–68.
Nara, H., S. Toyoda, and N. Yoshida (2007), Measurements of stable carbon isotopic composition of ethane and propane over the western North Pacific and eastern Indian Ocean: A useful indicator of atmospheric transport process, *J. Atmos. Chem.*, *56*(3), 293–314.
Nguyen, T. L., and J. R. Barker (2010), Sums and densities of fully coupled anharmonic vibrational states: A comparison of three practical methods, *Chem. – Eur. J.*, *114*(10), 3718–3730.
Nguyen, T. L., J. F. Stanton, and J. R. Barker (2010), A practical implementation of semi-classical transition state theory for polyatomics, *Chem. Phys. Lett.*, *499*(1–3), 9–15.
Nguyen, T. L., J. F. Stanton, and J. R. Barker (2011), Ab initio reaction rate constants computed using semiclassical transition-state theory: HO + H2 → H2O + H and Isotopologues, *Chem. – Eur. J.*, *115*(20), 5118–5126.
Pople, J. A., M. Head-Gordon, and K. Raghavachari (1987), Quadratic configuration interaction. A general technique for determining electron correlation energies, *J. Chem. Phys.*, *87*(10), 5968–5975.
Pozzer, A., J. Pollmann, D. Taraborrelli, P. Jöckel, D. Helmig, P. Tans, J. Hueber, and J. Lelieveld (2010), Observed and simulated global distribution and budget of atmospheric C2–C5 alkanes, *Atmos. Chem. Phys.*, *10*(9), 4403–4422.
Purvis, G. D., and R. J. Bartlett (1982), A full coupled-cluster singles and doubles model: The inclusion of disconnected triples, *J. Chem. Phys.*, *76*(4), 1910–1918.
Rudolph, J. (1995), The tropospheric distribution and budget of ethane, *J. Geophys. Res.*, *100*(D6), 11,369–11,381, doi:10.1029/95JD00693.
Rudolph, J. (2007), Gas chromatography–isotope ratio mass spectrometry, in *Volatile Organic Compounds in the Atmosphere*, edited by R. Koppmann, Blackwell Publ., Oxford, U. K., doi:10.1002/9780470988657.ch10.
Rudolph, J., and E. Czuba (2000), On the use of isotopic composition measurements of volatile organic compounds to determine the "photochemical age" of an air mass, *Geophys. Res. Lett.*, *27*(23), 3865–3868, doi:10.1029/2000GL011385.
Rudolph, J., D. C. Lowe, R. J. Martin, and T. S. Clarkson (1997), A novel method for compound specific determination of $\delta^{13}C$ in volatile organic compounds at ppt levels in ambient air, *Geophys. Res. Lett.*, *24*(6), 659–662, doi:10.1029/97GL00537.
Rudolph, J., E. Czuba, and L. Huang (2000), The stable carbon isotope fractionation for reactions of selected hydrocarbons with OH-radicals and its relevance for atmospheric chemistry, *J. Geophys. Res.*, *105*(D24), 29,329–29,346.
Rudolph, J., E. Czuba, A. L. Norman, L. Huang, and D. Ernst (2002), Stable carbon isotope composition of nonmethane hydrocarbons in emissions from transportation related sources and atmospheric observations in an urban atmosphere, *Atmos. Environ.*, *36*(7), 1173–1181.
Saito, T., U. Tsunogai, K. Kawamura, T. Nakatsuka, and N. Yoshida (2002), Stable carbon isotopic compositions of light hydrocarbons over the western North Pacific and implication for their photochemical ages, *J. Geophys. Res.*, *107*(D4), 4040, doi:10.1029/2000JD000127.
Saito, T., K. Kawamura, U. Tsunogai, T.-Y. Chen, H. Matsueda, T. Nakatsuka, T. Gamo, M. Uematsu, and B. J. Huebert (2009), Photochemical histories of nonmethane hydrocarbons inferred from their stable carbon isotope ratio measurements over east Asia, *J. Geophys. Res.*, *114*, D11303, doi:10.1029/2008JD011388.
Saito, T., O. Stein, U. Tsunogai, K. Kawamura, T. Nakatsuka, T. Gamo, and N. Yoshida (2011), Stable carbon isotope ratios of ethane over the North Pacific: Atmospheric measurements and global chemical transport modeling, *J. Geophys. Res.*, *116*, D02308, doi:10.1029/2010JD014602.
Schultz, M. G., et al. (2015), The global atmosphere watch reactive gases measurement network, *Elem.: Sci. Anthropocene*, *3*, 67.
Sellevåg, S. R., G. Nyman, and C. J. Nielsen (2006), Study of the carbon-13 and deuterium kinetic isotope effects in the Cl and OH reactions of CH_4 and CH_3Cl, *Chem. – Eur. J.*, *110*(1), 141–152.
Senosiain, J. P., C. B. Musgrave, and D. M. Golden (2001), Use of quantum methods with transition state theory: Application to H-atom metathesis reactions, *Chem. – Eur. J.*, *105*(9), 1669–1675.
Sharkey, P., and I. W. M. Smith (1993), Kinetics of elementary reactions at low temperatures: Rate constants for the reactions of OH with HCl (298 [gt-or-equal]*T*/*K* [gt-or-equal] 138), CH_4(298 [gt-or-equal]*T*/*K* [gt-or-equal] 178) and C_2H_6(298 [gt-or-equal]*T*/*K* [gt-or-equal] 138), *J. Chem. Soc., Faraday Trans.*, *89*(4), 631–637.
Simpson, I. J., M. P. Sulbaek Andersen, S. Meinardi, L. Bruhwiler, N. J. Blake, D. Helmig, F. S. Rowland, and D. R. Blake (2012), Long-term decline of global atmospheric ethane concentrations and implications for methane, *Nature*, *488*(7412), 490–494.
Stachnik, R. A., L. T. Molina, and M. J. Molina (1986), Pressure and temperature dependences of the reaction of hydroxyl radical with nitric acid, *J. Phys. Chem.*, *90*(12), 2777–2780.
Stein, O., and J. Rudolph (2007), Modeling and interpretation of stable carbon isotope ratios of ethane in global chemical transport models, *J. Geophys. Res.*, *112*, D14308, doi:10.1029/2006JD008062.
Talukdar, R. K., A. Mellouki, T. Gierczak, S. Barone, S. Y. Chiang, and A. R. Ravishankara (1994), Kinetics of the reactions of OH with alkanes, *Int. J. Chem. Kinet.*, *26*(10), 973–990.
Tanaka, N., Y. Xiao, and A. C. Lasaga (1996), Ab initio study on carbon kinetic isotope effect (KIE) in the reaction of CH4+cl•, *J. Atmos. Chem.*, *23*(1), 37–49.
Thompson, A., J. Rudolph, F. Rohrer, and O. Stein (2003), Concentration and stable carbon isotopic composition of ethane and benzene using a global three-dimensional isotope inclusive chemical tracer model, *J. Geophys. Res.*, *108*(D13), 4373, doi:10.1029/2002JD002883.
Tsunogai, U., N. Yoshida, and T. Gamo (1999), Carbon isotopic compositions of C2–C5 hydrocarbons and methyl chloride in urban, coastal, and maritime atmospheres over the western North Pacific, *J. Geophys. Res.*, *104*(D13), 16,033–16,039, doi:10.1029/1999JD900217.
Vereecken, L., D. R. Glowacki, and M. J. Pilling (2015), Theoretical chemical kinetics in tropospheric chemistry: Methodologies and applications, *Chem. Rev.*, *115*(10), 4063–4114.

Villà, J., J. C. Corchado, A. González-Lafont, J. M. Lluch, and D. G. Truhlar (1999), Variational transition-state theory with optimized orientation of the dividing surface and semiclassical tunneling calculations for deuterium and muonium kinetic isotope effects in the free radical association reaction $H+C_2H_4 \rightarrow C_2H_5$, *J. Phys. Chem. A*, *103*(26), 5061–5074, doi:10.1021/jp990970c.

Wagner, A. F. (2013), Improved multidimensional semiclassical tunneling theory, *Chem. – Eur. J.*, *117*(49), 13,089–13,100.

Xiao, Y., J. A. Logan, D. J. Jacob, R. C. Hudman, R. Yantosca, and D. R. Blake (2008), Global budget of ethane and regional constraints on U.S. sources, *J. Geophys. Res.*, *113*, D21306, doi:10.1029/2007JD009415.

Zabarnick, S., J. W. Fleming, and M. C. Lin (1988), Kinetics of hydroxyl radical reactions with formaldehyde and 1,3,5-trioxane between 290 and 600 K, *Int. J. Chem. Kinet.*, *20*(2), 117–129.

Zhao, Y., and D. Truhlar (2008), The M06 suite of density functionals for main group thermochemistry, thermochemical kinetics, noncovalent interactions, excited states, and transition elements: Two new functionals and systematic testing of four M06-class functionals and 12 other functionals, *Theor. Chem. Acc.*, *120*(1–3), 215–241.